A Study on Integrated SAR Processing and Geocoding by Means of Time-Domain Backprojection

Othmar Frey, Erich Meier, and Daniel Nüesch
Remote Sensing Laboratories
University of Zurich
CH-8057 Zurich, Switzerland
ofrey, meier, nuesch @geo.unizh.ch

Abstract— **Geocoded products of synthetic aperture radar data are of great interest for many applications. The conventional processing chain, which leads to geographically referenced synthetic aperture data consists of two main steps: first, the raw data are focused and, in a second step, the resulting single look complex image is geocoded to the favoured coordinate system.**

We investigate a time-domain backprojection approach that replaces the two steps, focusing and geocoding, by one algorithm leading directly to terrain-geocoded images.

The technique is evaluated with ENVISAT/ASAR image mode data. We assess the geolocation accuracy and the radiometric performance of dedicated point targets such as transponders and a corner reflector. In addition, we compare our findings with results from corresponding level 1 products processed at the European Space Agency (ESA), which were validated within the scope of ENVISAT/ASAR Cal/Val activities.

I. INTRODUCTION

Many end-users of synthetic aperture radar (SAR) data, especially in the field of geoscience, are above all interested in data that is geographically referenced – the so-called geocoded products. The increasing availability of accurate terrain and surface models enables a precise geographical localization of the data in map coordinates.

Various azimuth focusing techniques are available to transform SAR raw data to a single look complex (SLC) image such as the range-Doppler (RD) [1], the chirp scaling (CS) [2] [3] and the $\omega - k$ [4] algorithm. An up-to-date overview and comparison of the aforementioned algorithms is given in [5]. While these algorithms focus the SAR data in the one- or two-dimensional frequency domain the also well-known time-domain backprojection (TDBP) processing technique [6] [7] applies a completely different approach: the data are focused geometrically, i.e., in the time domain. This property gives rise to the possibility of backprojecting directly to a reconstruction surface of choice instead of being restricted to the natural range/azimuth geometry of conventional SAR imaging techniques. Thereby, the common two-step procedure of, first, focusing the SAR data and, second, geocoding the resulting SLC image to the desired map coordinates can be replaced by one integrated processing and geocoding algorithm. Key requirements for a successful application of this TDBP approach are accurate sensor positioning data and an accurate digital elevation model (DEM). These are, basically, the same requirements that must be met to obtain an accurately geocoded product from an SLC image. The geometric nature of TDBP has, besides one drawback in the form of high computational cost, a couple of advantages: influencing factors like atmospheric path delay, elevation antenna gain pattern, topography-induced variation of radar brightness may be accounted for during one processing stage, and, important for airborne SAR, full motion compensation is implemented with ease. And, by design, the TDBP algorithm is very suitable for processing SAR data in parallel.

In this paper, we assess the quality of the results of our integrated TDBP processing by analysing point targets. In particular, we use ENVISAT/ASAR image mode (IM) data of ESA transponders and a corner reflector. We compare our results with the corresponding level 1 products processed at ESA using the RD algorithm. The quality is assessed in terms of the geolocation accuracy as well as in terms of the radiometric performance. Quality measures defined for ENVISAT/ASAR Cal/Val help in order to quantify the radiometric performance of the impulse response of the transponders. The products of the different approaches are compared. In addition, we present an example of ENVISAT/ASAR IM data of a mountainous area processed by our TDBP processor using ENVISAT/DORIS precise orbit data and a digital elevation model.

II. SYSTEM MODEL

We briefly revise the system model of TDBP processing as described e.g. in [6] and rewrite it as a function of the three-dimensional position of a point in the reconstruction grid, which is the convenient form for our purpose. Reference [6] gives a comprehensive overview of TDBP and of fast backprojection techniques, which make use of approximations in order to reduce the computational burden. Another source which extensively discusses the subject is [7].

The following assumptions are made for a simplified description of the model: The sensor is mono-static (transmit and receive antenna are the very same). A vacuum propagation space is assumed and superposition shall apply since the ground is considered to be a collection of single-scattering objects. The usual start-stop approximation is supposed to be valid.

Assuming a linear sensor path the two-way response g for a single point target can be written as a function of the cylinder coordinates (ρ, θ, x) where ρ is the range distance at the point of closest approach between sensor and target, θ the elevation

angle, and x the azimuth position along the linear flight path:

$$g(R, x) = A(.) \cdot \sigma_0 \cdot \frac{p_{rc}(R - \sqrt{(x - x_0)^2 + \rho_0{}^2})}{(x - x_0)^2 + \rho_0{}^2} \ . \quad (1)$$

R is the range distance, $A(.)$ the amplitude function representing the antenna gain pattern, σ_0 the reflectivity of the point target at position (ρ_0, θ_0, x_0), and p_{rc} is the demodulated, range-compressed pulse.

The focused SAR signal s after TDBP at the range/azimuth position (ρ, x) is:

$$s(\rho, x) = \sum_{x'} g(R, x) \cdot R \cdot \exp(j2k_c R) \ , \quad (2)$$

where $R = \sqrt{(x' - x)^2 + \rho^2}$ is the range distance, x' the along-track integration parameter, $k_c = 2\pi f_c/c$ the central wavenumber corresponding to the carrier frequency f_c, and c is the speed of light. The exponential term brings the demodulated signal back to its original bandpass form.

Generalising to an arbitrary sensor path the two-way response g for a single point target at position $\vec{r}_0$ can be written as:

$$g(R, \vec{r}_S) = A(\vec{r}_S, \vec{r}_0) \cdot \sigma_0 \cdot \frac{p_{rc}(R - |\vec{r}_S - \vec{r}_0|)}{|\vec{r}_S - \vec{r}_0|^2} \ , \quad (3)$$

where $A(.)$ is the amplitude function representing the antenna gain pattern, σ_0 the reflectivity of the point target at position $\vec{r}_0$, p_{rc} the demodulated and range-compressed pulse, $\vec{r}_S$ the three-dimensional position vector of the sensor, and R the range distance.

In order to be able to back-project the data directly to a three-dimensional reconstruction grid consisting of the grid points $\vec{r}_i$ we want to express the back-projected signal s not as a function of the range distance ρ and the sensor position $\vec{r}_S$, but as a function of the grid point $\vec{r}_i$:

$$s(\vec{r}_i) = \sum_{j=a(\vec{r}_i)}^{b(\vec{r}_i)} g(|\vec{r}_i - \vec{r}_{S_j}|, \vec{r}_{S_j}) \cdot |\vec{r}_i - \vec{r}_{S_j}| \cdot \exp(j2k_c|\vec{r}_i - \vec{r}_{S_j}|) \ , \quad (4)$$

where a and b are the indices of the first or last sensor position, respectively, the echo of which still contributes to the grid position $\vec{r}_i$. This means that we sum up the contributions from those sensor positions $\vec{r}_{S_j}$ which build the synthetic aperture for the grid position $\vec{r}_i$. Note that a and b vary as a function of the grid position $\vec{r}_i$.

Equation (4) builds the foundation of the TDBP algorithm as it is applied to the data presented in the paper at hand. Since the actual signal is sampled at discrete points in time an appropriate interpolation procedure has to be implemented in order to retrieve the range-compressed data at the correct range distances.

Fig. 1 depicts the processing chain of integrated azimuth-focusing and geocoding by means of TDBP.

III. DATA

The ENVISAT/ASAR IM data used for the validation of the integrated TDBP approach includes two scenes of Flevoland, The Netherlands, descending orbit 3540, beam IS7 and ascending orbit 3547, beam IS1. Each of them contains
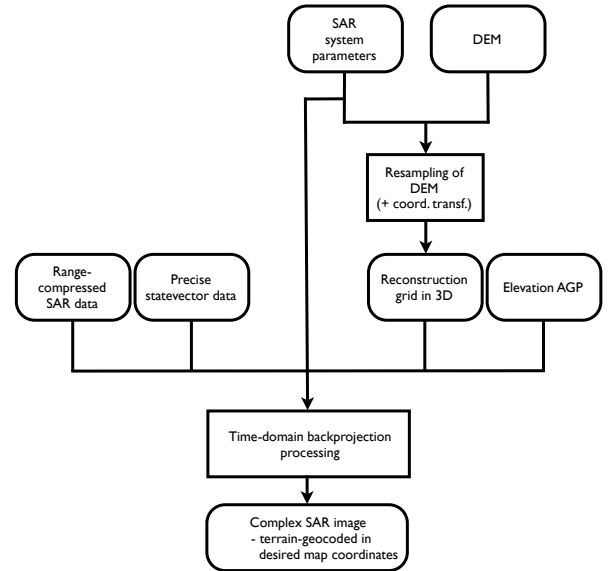
Fig. 1. Flow diagram of the integrated processing and geocoding approach using time-domain backprojection.

the two ESA transponders [8] in Swifterbant and Zwolle, respectively. Another three scenes containing a corner reflector deployed in Dübendorf, Switzerland, were investigated. These are descending orbit 7863, beam IS1, descending orbit 7963, beam IS6, and descending orbit 8092, beam IS2.

The position of the corner reflector is known very accurately on the order of centimeters and below. An internal delay uncertainty of about 10 nanoseconds [9] biases the predicted position of the transponders mainly in slant-range direction.

In order to be able to compare the results of the TDBP and RD processing, care has been taken with respect to equal processing boundary conditions. All ENVISAT/ASAR IM data sets presented throughout this paper were processed using the following parameters: both, range and azimuth spectra have been windowed by a Hamming window with a coefficient of 0.75. Further, a fraction of 80% of the total Doppler bandwidth has been processed.

Prerequisites for a successful geocoding without ground control points are precise sensor positioning data, which is given for ENVISAT/ASAR, and an accurate DEM. ENVISAT/DORIS precise orbit data (DOR_VOR_AX) build the source for accurate sensor positioning. State vectors are provided at intervals of 60 s. According to [10] the total absolute orbit error is as low as 10 cm RMS and the absolute radial error even lower than 5 cm RMS. Interpolating the intermediate state vectors using a higher-order polynomial certainly deteriorates the accuracy, but the errors are expected to remain small compared to the resolution capabilities of the ASAR system or the accuracy of a DEM.

IV. VALIDATION

The output of the TDBP processor is validated with respect to its radiometric performance and its geolocation accuracy with the help of the aforementioned ENVISAT/ASAR IM data. We have chosen this product since it is well calibrated and documented and because there are reference products

available for comparison. The radiometric performance is assessed by calculating and comparing various quality measures from the impulse response of the two ESA transponders. The same transponders and the corner reflector, which was situated on an airfield in Dübendorf during the ENVISAT/ASAR Cal/Val period, are used for the validation of the geometric fidelity of the data processed by the TDBP algorithm. Most recent instrument calibration files were used which contain refined sampling window start time (SWST) bias values validated in [11]. In addition, the azimuth "bistatic" bias [12] has been accounted for within the TDBP processing procedure: Radar echos of ENVISAT/ASAR are annotated to the *receive* time t_R. Since the platform moves between transmitting and receiving a pulse the azimuth time corresponding to the Doppler centroid frequency t_{DC} is:

$$t_{DC} = t_R - 1/2 \cdot t_F \qquad (5)$$

For ENVISAT/ASAR IM data this azimuth bias of one half of the fast-time t_F varies slightly ($< 4\%$) within one beam and amounts to 20 - 25 m depending on the imaged swath.

It is stressed that the proposed procedure does not make use of positional refinements by incorporating ground control points. The geolocation is established only by precise state vectors and a digital elevation model.

A. Geolocation Accuracy

The geolocation accuracy has been determined and is presented in both, local map coordinates and range/azimuth geometry – the latter for the sake of comparability. The difference between the true ("predicted") position of the point target and the measured position in the geocoded image has been calculated. In order to obtain the correct prediction for the geolocation of a transponder the internal delay has to be taken into account [13]. From the known coordinates of the transponder the position of the sensor is searched at the point where the following equation is satisfied:

$$f_{DC} = \frac{2 \cdot \left(\vec{V}_S - \vec{V}_P \right) \left(\vec{P} - \vec{S} \right)}{\lambda \cdot R} \ , \qquad (6)$$

where f_{DC} is the Doppler centroid frequency, $\vec{P}$ the position of the target on the reconstruction surface, $\vec{V}_P$ the velocity of the target (= $\vec{0}$ for ECR coordinates), $\vec{S}$ the sensor position, $\vec{V}_S$ the sensor velocity, λ the wavelength, and $R = |\vec{P} - \vec{S}|$ is the range distance. Having the sensor position the transponder delay is added to the real range delay and the same equation is solved for a point on the local map plane – the predicted transponder position.

To enable a direct comparison between the geolocation validation of point target positions in SLC images processed at ESA (see [12]), on the one hand, and the respective results from TDBP processing, on the other hand, the measured displacements have been converted to range/azimuth geometry by the following procedure: For the predicted point target position the appropriate sensor position satisfying equation (6) is searched for, given the Doppler centroid frequency. The difference vector in Easting/Northing (E/N) of local map coordinates is then converted to global Cartesian coordinates (WGS84) and, after that, projected onto the unity slant-range vector or the unity velocity vector corresponding to the

satellite position found beforehand. In Table I the results of the geolocation validation of TDBP processing, transformed into range/azimuth geometry, are summarized.

Orbit	Beam	Predicted - measured pos.		Type & Location
		ΔR [m]	ΔA [m]	
3540	IS7 D	-2.3	7.0	TP, Swifterbant, NL
3540	IS7 D	6.4	5.8	TP, Zwolle, NL
3547	IS1 A	-2.4	2.6	TP, Swifterbant, NL
3547	IS1 A	5.9	3.5	TP, Zwolle, NL
7863	IS1 D	4.6	1.7	CR, Dübendorf, CH
7963	IS6 D	4.5	2.3	CR, Dübendorf, CH
8092	IS2 D	5.7	1.5	CR, Dübendorf, CH

TABLE I

ABSOLUTE POSITIONING ACCURACY [Δ R = RANGE / Δ A = AZIMUTH] OF MEASURED POINT TARGETS GIVEN IN RANGE/AZIMUTH GEOMETRY. CR = CORNER REFLECTOR, TP = TRANSPONDER.

Orbit	Beam	Predicted - measured pos.		Type & Location
		ΔE [m]	ΔN [m]	
3540	IS7 D	2.2	-7.4	TP, Swifterbant, NL
3540	IS7 D	-10.0	-4.3	TP, Zwolle, NL
3547	IS1 A	-8.7	0.5	TP, Swifterbant, NL
3547	IS1 A	17.2	7.8	TP, Zwolle, NL
7863	IS1 D	-16.5	1.9	CR, Dübendorf, CH
7963	IS6 D	-7.2	-1.2	CR, Dübendorf, CH
8092	IS2 D	-16.4	2.0	CR, Dübendorf, CH

TABLE II

ABSOLUTE POSITIONING ACCURACY [$\Delta E/\Delta N$] OF MEASURED POINT TARGETS GIVEN IN THE RESPECTIVE LOCAL MAP COORDINATES (E/N). CR = CORNER REFLECTOR, TP = TRANSPONDER.

All range differences are smaller than the nominal range pixel spacing (7.804 m). In azimuth direction, the maximum difference for a transponder has about the size of two azimuth pixels. However, the azimuth location errors for the Dübendorf corner reflector, where no potential delay uncertainty is given, are all on a sub-pixel level. The achieved geolocation accuracy for the corner reflector is comparable to the one reported in [12] where, for the corner reflector in Dübendorf, range differences of 2.0 - 2.6 m and azimuth differences of 1.4 - 1.7 m were found evaluating the same scenes (orbits 7863, 7963 and 8092). Note that in [12] the geometric validation is done in range/azimuth geometry whereas we originally processed the data to map coordinates.

Depending on the local incidence angle, the position and attitude of the sensor, the geolocation error in range/azimuth geometry presented in Table I may translate to greater errors when given in map coordinates as can be seen in Table II where the same errors are displayed in E/N of local map coordinates.

B. Radiometric Performance

The radiometric performance is evaluated with the help of the two ESA transponders. Appropriate ENVISAT/ASAR IM scenes were processed via TDBP and the output was compared with the corresponding, RD-processed level 1 (IMS) products. In order to ease the comparison with the IMS data the range-compressed data was back-projected onto a reconstruction grid that is equivalent to the natural slant-range geometry of single look complex images.

For a quantification of ENVISAT/ASAR imagery numerous quality measures had already been defined within the scope of ASAR Cal/Val some of which are used here to assess the radiometric performance. In particular these are:

1) Spatial resolution
2) Peak to side lobe ratio (PSLR)
3) Spurious side lobe ratio (SSLR)
4) Integrated side lobe ratio (ISLR)
5) Ratio of total power to peak height (TPPR)

For a detailed description of these quality measures the reader is referred to [14] and [15].

Transponder location		Swifterbant, NL		
Orbit & beam		3540 IS7 D		3547 IS1 A
Processing algorithm		TDPB	RD	TDPB
Res. (range)	[m]	9.3	9.3	9.3
Res. (azimuth)	[m]	4.5	4.8	5.5
PSLR (range)	[dB]	-20.1	-19.9	-19.9
PSLR (azimuth)	[dB]	-28.8	-28.9	-27.2
SSLR	[dB]	-27.6	-27.9	-26.4
ISLR	[dB]	-14.3	-14.3	-12.6
TPPR	[dB]	26.3	26.9	26.1
Transponder location		Zwolle, NL		
Orbit & beam		3540 IS7 D		3547 IS1 A
Processing algorithm		TDPB	RD	TDPB
Res. (range)	[m]	9.3	9.3	9.3
Res. (azimuth)	[m]	4.5	4.8	5.5
PSLR (range)	[dB]	-20.1	-20.2	-20.2
PSLR (azimuth)	[dB]	-28.1	-28.1	-26.4
SSLR	[dB]	-27.9	-28.1	-27.5
ISLR	[dB]	-14.3	-14.3	-13.7
TPPR	[dB]	26.3	26.9	26.1

TABLE III

RADIOMETRIC PERFORMANCE. QUALITY MEASURES CALCULATED FROM THE IMPULSE RESPONSE OF TRANSPONDERS.

In Table III the results from the analysis of the impulse response function (IRF) of the transponders in Swifterbant and Zwolle are provided for both, TDBP and RD processing at beam IS7 of orbit 3540, and for TDBP only at beam IS1 of orbit 3547. A plot of the IRF analysis including range and azimuth cuts through the peak of the IRF after TDBP processing is given in Fig. 2. The respective analysis of the data processed at ESA using the RD algorithm is depicted in Fig. 3. As can be seen from the results presented in the tables and plots, the values for the quality measures are in accordance with each other; the lower resolution in azimuth direction for orbit 3547, beam IS1 is due to the lower pulse repetition frequency implemented at this beam.

Spectral plots of the TDBP-processed Swifterbant transponder area are provided in Fig. 4 including the two-dimensional magnitude spectrum of the area as well as the magnitude spectrum of the IRF cuts in range (fast-time) and azimuth (slow-time).

V. DATA IN RUGGED TERRAIN

Fig. 5 depicts a SAR image of the Lake of Zug, Switzerland, and its surroundings processed directly to local map coordinates (E/N) by TDBP. The coordinates of the points in the reconstruction grid are interpolated from a digital terrain model (Swiss DHM25, original horizontal grid spacing: 25 m). The scene has been acquired by ENVISAT/ASAR on
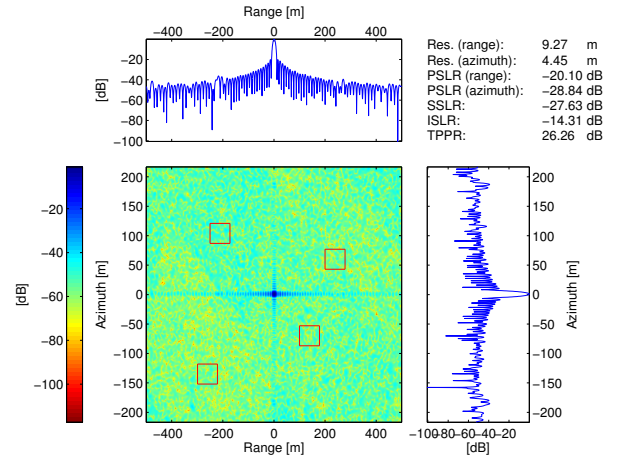
Fig. 2. Transponder Swifterbant, ENVISAT/ASAR orbit 3540 IS7 D, **time-domain backprojection processing**. Res. = resolution, PSLR = peak to side lobe ratio, SSLR = spurious side lobe ratio, ISLR = integrated side lobe ratio, TPPR = total peak to power ratio.
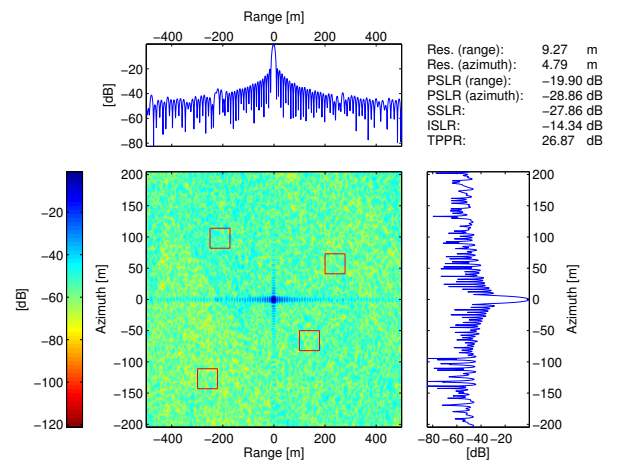
Fig. 3. Transponder Swifterbant, ENVISAT/ASAR orbit 3540 IS7 D, **range-Doppler processing** (ESA). Res. = resolution, PSLR = peak to side lobe ratio, SSLR = spurious side lobe ratio, ISLR = integrated side lobe ratio, TPPR = total peak to power ratio.

orbit 7963 at beam IS6 D in image mode. ENVISAT/DORIS precise orbits are again used for accurate sensor positioning.

At the northeastern end of the Lake of Zug the city of Zug is visible. The prominent, bright features at the southwestern end of the lake stem from the steep slopes of the Rigi Mountain the surface normals of which point towards the sensor.

VI. CONCLUSIONS AND OUTLOOK

By analysing the impulse response of transponders and a corner reflector we have shown that the quality of the results of integrated processing and geocoding by means of time-domain backprojection (TDBP) processing matches the quality of the level 1 image mode (IMS) data products obtainable from ESA. The achieved geolocation accuracy is surprisingly good and conforms with the findings in [11]. This accuracy is obtained "out of the box", i.e. no ground control points were used. Further, the radiometric performance was found to be equivalent for both of the compared approaches, TDBP and RD processing.

The presented approach replaces the two steps, focusing
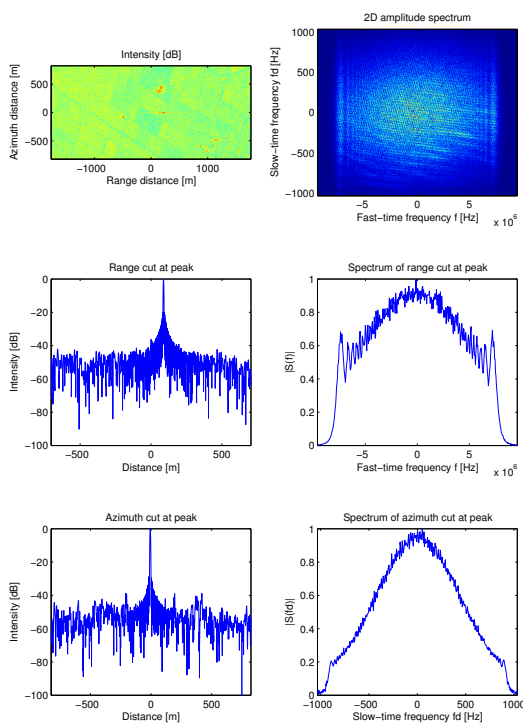
Fig. 4. Transponder Swifterbant, ENVISAT/ASAR orbit 3540 IS7 D, time-domain backprojection processing. The scene is centered at the true transponder position. Note the shift of the peak in range due to the transponder delay.

Fig. 5. Integrated processing and geocoding of SAR data of the area around Lake of Zug, Switzerland, by time-domain backprojection. Local map coordinates (E/N). Data: ENVISAT/ASAR IM, orbit 7963, beam IS6. DEM: Swiss DHM25.

and geocoding, by one algorithm leading directly to terrain-geocoded images. The reconstruction grid can be chosen freely within the boundaries of the given sampling constraints. Thus, a region of interest can directly be selected in local map coordinates and the corresponding extract from the range-compressed data is then processed without having to focus the whole data set.

We intend to enhance our TDBP approach by further exploiting its geometric nature. Potential improvements may include a radiometric correction for topography-induced variation of radar brightness and atmospheric corrections.

ACKNOWLEDGMENT

REFERENCES

[1] J. C. Curlander and R. N. McDonough, *Synthetic Aperture Radar - Systems and Signal Processing*. New York: John Wiley & Sons, 1991.

[2] R. K. Raney, H. Runge, R. Bamler, I. G. Cumming, and F. Wong, "Precision SAR Processing Using Chirp Scaling," *IEEE Transactions on Geoscience and Remote Sensing*, vol. 32, no. 4, pp. 786–799, 1994.

[3] A. Moreira and Y. Huang, "Airborne SAR Processing of Highly Squinted Data Using a Chirp Scaling Approach with Integrated Motion Compensation," *IEEE Transactions on Geoscience and Remote Sensing*, vol. 32, no. 5, pp. 1029–1040, 1994.

[4] C. Cafforio, C. Prati, and F. Rocca, "SAR Data Focusing Using Seismic Migration Techniques," *IEEE Transactions on Aerospace and Electronic Systems*, vol. 27, no. 2, pp. 194–207, 1991.

[5] I. G. Cumming and F. H. Wong, *Digital Processing of Synthetic Aperture Radar Data: Algorithms and Implementation*. Boston, London: Artech House Inc., 2005.

[6] L. M. H. Ulander, H. Hellsten, and G. Stenström, "Synthetic-Aperture Radar Processing Using Fast Factorized Back-Projection," *IEEE Transactions on Aerospace and Electronic Systems*, vol. 39, no. 3, pp. 760–776, July 2003.

[7] M. Soumekh, *Synthetic Aperture Radar Signal Processing: with MAT-LAB Algorithms*. John Wiley & Sons, 1999.

[8] H. Jackson, I. Sinclair, and S. Tam, "ENVISAT/ASAR Precision Transponders," in *CEOS SAR Workshop 1999*, Toulouse, Oct. 1999.

[9] D. Small, J. Holzner, H. Raggam, D. Kosmann, and A. Schubert, "Geometric performance of ENVISAT ASAR products," in *IGARSS '03, International Geoscience and Remote Sensing Symposium*, vol. 2, pp. 1121–1123, 2003.

[10] M. Otten and H. Boomkamp, "Estimation of the Absolute Orbit Accuracy of Envisat," European Space Operations Centre (ESOC), Robert-Bosch Strasse 5, D-64283 Darmstadt, Tech. Rep., 2003.

[11] D. Small, B. Rosich, E. Meier, and D. Nüesch, "Geometric Calibration and Validation of ASAR Imagery," in *CEOS SAR Workshop 2004*, Ulm, May 2004.

[12] D. Small, B. Rosich, A. Schubert, E. Meier, and D. Nüesch, "Geometric Validation of Low and High-Resolution ASAR Imagery," Submitted to Proc. ENVISAT/ERS Symposium, Salzburg, Sep. 2004.

[13] D. Small, A. Schubert, U. Krüttli, E. Meier, and D. Nüesch, "Preliminary Validation of ASAR Geometric Accuracy," in *Proceedings of ENVISAT Validation Workshop*, ESA-ESRIN, Frascati, Dec. 2002.

[14] ASAR-Cal/Val-Team, "Quality Measurements Definition for ASAR Level 1 Products," ESA, Tech. Rep. Iss. 1, Mar. 2002.

[15] B. Rosich and P. Meadows, "Absolute Calibration of ASAR Level 1 Products Generated with PF-ASAR," ESA, Tech. Rep. Iss. 1 rev. 5, Oct. 2004.